Journal of Power Sources 196 (2011) 4451–4457

Contents lists available at ScienceDirect

Journal of Power Sources

journal homepage: www.elsevier.com/locate/jpowsour

Effect of carbon deposition by carbon monoxide disproportionation on electrochemical characteristics at low temperature operation for solid oxide fuel cells

Hirofumi Sumi[a], Yi-Hsuan Lee[a], Hiroki Muroyama[a], Toshiaki Matsui[a], Motohisa Kamijo[b], Shin Mimuro[b], Mitsugu Yamanaka[b], Yasushi Nakajima[b], Koichi Eguchi[a,*]

[a] Department of Energy and Hydrocarbon Chemistry, Graduate School of Engineering, Kyoto University, Nishikyo-ku, Kyoto, 615-8510, Japan
[b] EV System Laboratory, Nissan Research Center, Nissan Motor Co., Ltd., Yokosuka, Kanagawa, 237-8523, Japan

ARTICLE INFO

Article history:
Received 22 November 2010
Received in revised form 7 January 2011
Accepted 20 January 2011
Available online 26 January 2011

Keywords:
Carbon deposition
CO dispropotionation
Methane cracking
Nickel–yttria stabilized zirocnia (Ni–YSZ) anode
Solid oxide fuel cell (SOFC)

ABSTRACT

The deterioration by carbon deposition was evaluated for electrolyte- and anode-supported solid oxide fuel cells (SOFCs) in comparison with carbon monoxide disproportionation and methane cracking. The polarization resistance of the nickel–yttria stabilized zirconia (Ni–YSZ) anode increased with a rise in CO concentration in H_2–CO–CO_2 mixture for the electrolyte-supported cells at 923 K. The resistance, however, did not change against CO concentration for the anode-supported cells. In a methane fuel with a steam/carbon (S/C) ratio of 0.1, the cell performance decreased for both of the cells at 1073 K. A large amount of agglomerated amorphous carbon was deposited from the anode surface to the interface between the anode and the electrolyte after power generation at S/C = 0.1 in methane fuel. On the other hand, the crystalline graphite was deposited only at the anode surface for the anode-supported cell after power generation in CO–CO_2 mixture. These results suggest that the reaction rate of CO disproportionation is faster than that of methane cracking. The deposited carbon near the anode/electrolyte interface caused the increase in the polarization resistance.

1. Introduction

Solid oxide fuel cells (SOFCs) are expected as power generation systems with high energy conversion efficiency. One of SOFCs' advantages is the possibility of power generation by direct fuel supplies of carbon monoxide and hydrocarbon. Recently, two approaches have been proposed to decrease the operating temperature of SOFCs from 1073–1273 K to 773–973 K. One approach is to use new materials that have high ionic conductivity at lower temperatures, such as $LaGaO_3$ [1] and Gd (or Sm)-doped CeO_2 [2], as the electrolyte, and the other is to thin down the electrolyte made of conventional materials [3–7]. For instance, the power density as high as 0.4 W cm^{-2} was successful to be obtained at 773 K for microtubular-type SOFCs with Gd-doped ceria thin-film electrolyte [5–7]. The SOFCs operated at low temperatures are suitable for portable power sources and auxiliary power units of vehicles.

Hydrocarbon fuels are generally supplied with internal and/or external steam reforming for SOFCs. Solid carbon is expected to be deposited by cracking reaction at low steam/carbon (S/C) ratios in the hydrocarbon fuels, which causes the deterioration of the anode performance due to deactivation of nickel catalyst and inhibition of fuel diffusion [8–15]. The cracking reaction of hydrocarbon tends to proceed at high temperatures in thermodynamic equilibrium [11,16]. On the other hand, we should also pay attention to the carbon deposition by disproportionation reaction of carbon monoxide at low temperatures [16,17]. The carbon deposition was actually confirmed with a supply of CO-rich gas for Ni-Fe and Ni/SiO_2 catalysts at 673–923 K [17–21]. It was reported that carbon dioxide reforming of methane is possible to cause the carbon deposition at low temperatures because of high CO concentration in reformate gas [22]. Under SOFC operation, the anodic overpotential increased with a rise in CO concentration in H_2–CO mixture at low temperatures [15,23–25]. However, water is generally contained in reformate gas, syngas, biogas and so on. The reaction system becomes complicated for the fuels containing water due to the occurrence of water gas shift reaction. The effects of the carbon deposition by CO disproportionation on the electrochemical characteristics have been insufficient to be investigated under SOFC operation.

In this study, power generation tests were conducted at relatively low temperature (923 K) as a function of H_2/CO ratios in H_2–CO–H_2O and H_2–CO–CO_2 mixtures to investigate the influences

* Corresponding author. Tel.: +81 0 75 383 2519; fax: +81 0 75 383 2520.
E-mail address: eguchi@scl.kyoto-u.ac.jp (K. Eguchi).

0378-7753/$ – see front matter © 2011 Elsevier B.V. All rights reserved.
doi:10.1016/j.jpowsour.2011.01.061

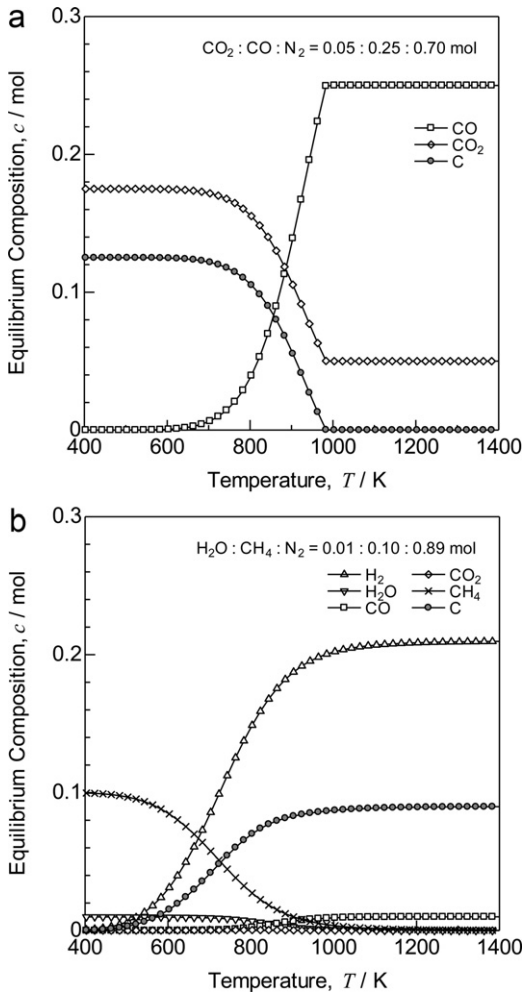

Fig. 1. Thermodynamic equilibrium compositions in (a) CO_2:CO:N_2 = 0.05:0.25:0.70 and (b) H_2O:CH_4:N_2 = 0.01:0.10:0.89 mol.

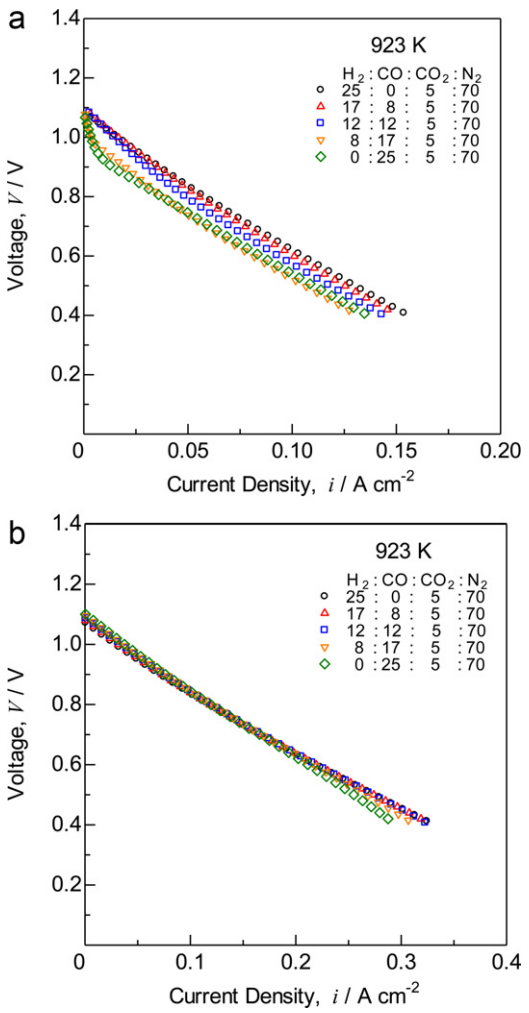

Fig. 2. Current–voltage characteristics for the (a) electrolyte- and (b) anode-supported cells with a supply of H_2–CO–CO_2 mixture at 923 K.

of CO disproportionation and water gas shift reactions on electrochemical characteristics. Electrolyte- and anode-supported cells were used to evaluate the effect of the anode thickness. The power generation tests were also conducted for a low S/C ratio of methane at 1073 K. The anodes after power generation were observed with field emission-scanning electron microscopy (FE-SEM) and Raman spectroscopy to compare the crystallinity, morphology and distribution of deposited carbon by CO disproportionation and methane cracking.

2. Experimental

Two types of electrolyte- and anode-supported cells were used in this study. Electrolyte, anode and cathode were $(Y_2O_3)_{0.08}$–$(ZrO_2)_{0.92}$ (YSZ), Ni–YSZ and $(La_{0.6}Sr_{0.4})(Co_{0.2}Fe_{0.8})O_3$ (LSCF), respectively. For the electrolyte-supported cells, the Ni–YSZ slurry was printed on a side of YSZ disk (thickness: 200 μm, diameter: 20 mm), and the $Ce_{0.8}Sm_{0.2}O_{1.9}$ (SDC) slurry was painted on the opposite side of the YSZ disk to prevent the reaction between the YSZ electrolyte and the LSCF cathode. The Ni–YSZ and SDC layers were co-sintered at 1573 K for 5 h in air. Then, the LSCF slurry was printed on SDC barrier layer, and was calcined at 1173 K for 5 h in air. The thickness and diameter of electrodes were 30 μm and 6 mm, respectively. For the anode- supported cells, the YSZ electrolyte and $Ce_{0.8}Y_{0.2}O_{1.9}$ (YDC) barrier layers (thickness: 10 μm) were formed on Ni–YSZ anode substrate (thickness: 500 μm, diameter: 20 mm), and were co-sintered at 1573 K for 5 h in air. Then, the LSCF cathode (thickness: 30 μm, diameter: 17 mm) was calcined on YDC barrier layer at 1173 K for 5 h in air.

In power generation tests, the mixtures of H_2:CO:H_2O (or CO_2):N_2 = 25 − x:x:y:75 − y and pure O_2 were supplied to anode and cathode at 923 K, respectively. The total gas flow rate was 100 mL min^{-1} in every condition. The water or carbon dioxide was supplied to define an oxygen partial pressure in the anode chamber. The changes in the species (H_2O, CO_2) and the composition (y) were to investigate the effects of carbon deposition and water gas shift reaction. Current–voltage (i–V) characteristics were evaluated with potentiostat/galvanostat (Solartron Analytical 1470E). The ac impedance was measured under open circuit voltage (OCV) in the frequency range from 100 kHz to 0.1 Hz with an impedance analyzer (Solartron Analytical 1455A) at the anode-reference electrode and the anode–cathode for the electrolyte- and anode-supported cells, respectively. The compositions of exhaust gases from the anode chamber were analyzed with thermal conductivity detector (TCD) in micro gas chromatography (Valian 490-GC; H_2, N_2, CH_4, CO: Molecular Sieve 5A column, CO_2: Porapak U column) for the anode-supported cells. The power generation tests were also conducted in the mixture of H_2O:CH_4:N_2 = 1:10:89 at 1073 K. The durability was evaluated for 20 h in the mixtures of CO_2:CO:N_2 = 5:25:70 at 923 K and H_2O:CH_4:N_2 = 1:10:89 at 1073 K. The anodes after the durability tests were observed with FE-SEM (Carl Zeiss NVision40) and Raman spectroscope (Horiba Jobin Yvon LabRAM HR-800). An accelerating voltage of FE-SEM was 2 kV to

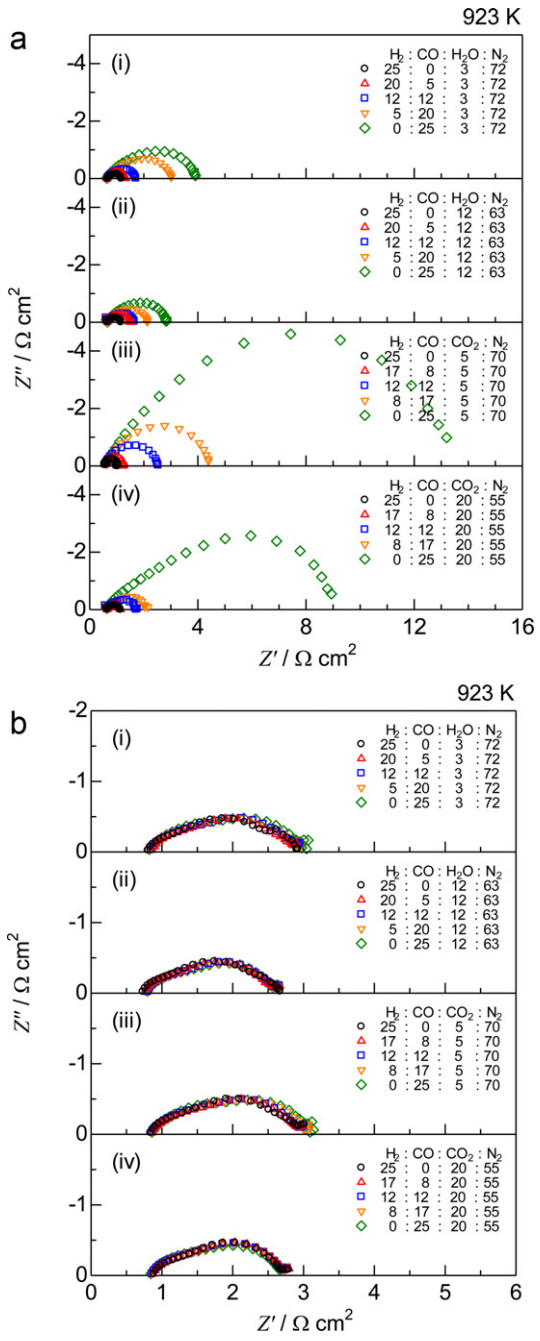

Fig. 3. AC impedance spectra for the (a) electrolyte- and (b) anode-supported cells with a supply of H_2–CO–H_2O (or CO_2) mixture at 923 K. The impedances were measured between the anode and reference electrode for the electrolyte-supported cell, and between the anode and cathode for anode-supported cell.

obtain the secondary electron and backscattered electron images. Raman spectra were measured in air with the use of a 514.5 nm Ar^+ laser. Equilibrium compositions were calculated by HSC Chemistry 5.11 (Outokumpu).

3. Results and discussion

Fig. 1 shows the temperature dependence of thermodynamic equilibrium compositions in (a) CO_2:CO:N_2 = 0.05:0.25:0.70 mol and (b) H_2O:CH_4:N_2 = 0.01:0.10:0.89 mol. In CO–CO_2 mixture, carbon can be deposited by disproportionation of carbon monoxide called as the Boudouard reaction.

$$2CO \rightarrow CO_2 + C \quad \Delta H_{298\,K} = -172\,kJ\,mol^{-1} \qquad (1)$$

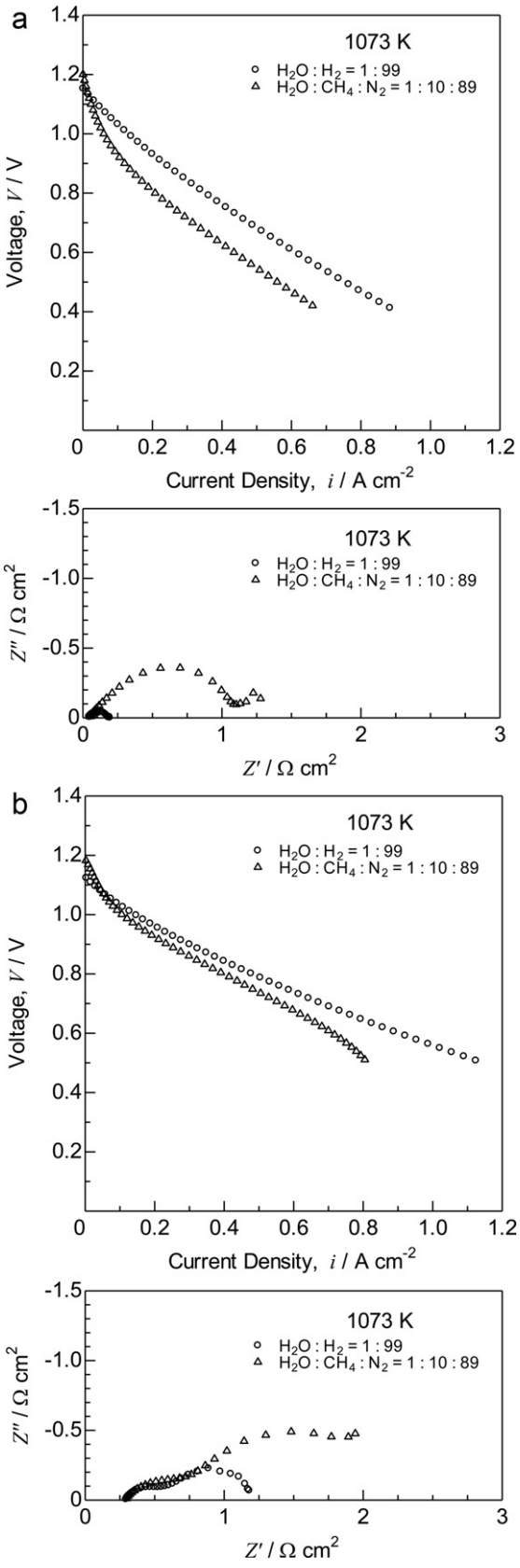

Fig. 4. Current–voltage characteristics and AC impedance spectra for the (a) electrolyte- and (b) anode-supported cells with supplies of H_2O–H_2 and H_2O–CH_4 mixtures at 1073 K. The impedances were measured between the anode and reference electrode for the electrolyte-supported cell, and between the anode and cathode for anode-supported cell.

Table 1
Gas production of H_2, CO and CO_2 (mL min^{-1}) and H_2/CO ratios in anode exhaust gas for the anode-supported cells at 0, 142 mA and 923 K with supplies of H_2:CO:H_2O or CO_2:N_2 = 25 − x:x:y:75 − y. The calculated values are in equilibrium.

H_2–CO–H_2O mixture (y = 3)							H_2–CO–CO_2 mixture (y = 5)						
x		H_2	H_2O	CO	CO_2	H_2/CO	x		H_2	H_2O	CO	CO_2	H_2/CO
0	Calc.	25.0	3.0	0.0	0.0	∞	0	Calc.	20.5	4.0	3.4	1.3	6.02
	0 mA	22.3	–	0.0	0.0	∞		0 mA	16.4	–	2.9	2.1	4.21
	142 mA	21.3	–	0.0	0.0	∞		142 mA	15.7	–	2.4	2.5	4.61
5.0	Calc.	19.7	2.5	3.7	0.9	5.32	8.3	Calc.	13.7	2.2	9.6	3.2	1.43
	0 mA	18.2	–	4.5	1.0	4.04		0 mA	11.9	–	9.1	4.3	1.18
	142 mA	17.6	–	4.4	1.2	4.00		142 mA	11.4	–	8.4	5.1	1.21
12.5	Calc.	12.9	1.8	8.8	2.5	1.47	12.5	Calc.	10.1	1.9	11.8	4.4	0.86
	0 mA	12.9	–	10.4	2.1	1.24		0 mA	9.2	–	12.2	5.2	0.70
	142 mA	12.2	–	10.1	2.9	1.21		142 mA	8.8	–	11.4	6.2	0.71
20.0	Calc.	6.5	1.3	12.2	4.8	0.53	16.7	Calc.	5.8	1.3	13.9	6.2	0.42
	0 mA	7.5	–	16.7	2.7	0.45		0 mA	6.5	–	15.5	5.9	0.39
	142 mA	6.8	–	16.4	3.8	0.41		142 mA	6.2	–	14.5	7.0	0.40
25.0	Calc.	2.4	0.6	14.2	6.6	0.17	25.0	Calc.	0.0	0.0	16.7	9.1	0.00
	0 mA	3.5	–	21.2	2.8	0.17		0 mA	0.0	–	22.0	7.0	0.00
	142 mA	2.4	–	20.8	4.2	0.12		142 mA	0.0	–	20.8	8.5	0.00

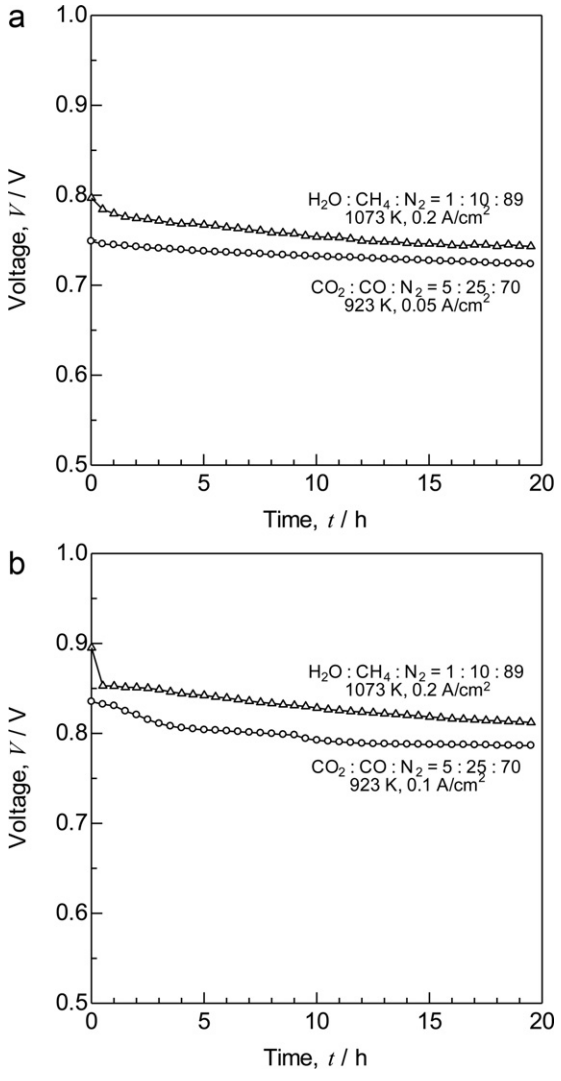

Fig. 5. Time courses of cell voltage for the (a) electrolyte- and (b) anode-supported cells with supplies of CO_2–CO mixture at 923 K and H_2O–CH_4 mixture at 1073 K.

This reaction tends to proceed at low temperatures as shown in Fig. 1(a). Carbon will not be deposited above 1173 K in equilibrium via this reaction. On the other hand, carbon is deposited by methane cracking at low S/C ratios from methane fuel.

$$CH_4 \rightarrow 2H_2 + C \quad \Delta H_{298\,K} = +19\,kJ\,mol^{-1} \tag{2}$$

This reaction tends to proceed at high temperatures as shown in Fig. 1(b), whereas the Boudouard reaction favors low temperatures.

Next, the *i*–*V* and ac impedance characteristics were evaluated in H_2:CO:H_2O (or CO_2): N_2 = 25 − x:x:y:75 − y at 923 K. In the cases of y = 3 (H_2O) and 5 (CO_2), carbon can be deposited at x > 16.7 in equilibrium. Fig. 2 shows the *i*–*V* characteristics for the (a) electrolyte- and (b) anode-supported cells with a supply of H_2–CO–CO_2 mixture at y = 5 and 923 K. The slopes of *i*–*V* curves became steep at low current density and x > 16.7 for the electrolyte-supported cells, which suggests the inhibition of electrode reaction by carbon deposition. The area specific resistance (ASR) evaluated from the *i*–*V* curve at a region of 0.05–0.1 A cm^{-2} was *ca.* 5 Ω cm^2 in every condition of Fig. 2(a). No dependence of the ASR on the fuel composition was caused by the promotion of electrochemical oxidation of not only hydrogen and carbon monoxide but also deposited carbon at high current densities. On the other hand, the slopes of *i*–*V* curves were almost the same at low current density in every condition for the anode-supported cells. The ASR value was evaluated to be *ca.* 3 Ω cm^2 in every condition of Fig. 2(b), which was smaller than that for electrolyte-supported cell. The slopes at high current density became steep with an increase in x, because the diffusion resistance of carbon monoxide was larger than that of hydrogen in the thick anode layer for the anode-supported cells.

Fig. 3 shows the ac impedance spectra with supplies of H_2–CO–H_2O(or CO_2) mixtures at OCV and 923 K. The total resistance for the electrolyte-supported cell was difference from the ASR evaluated from the *i*–*V* curve, because the impedance was measured between the anode and reference electrode in Fig. 3(a). The impedance arc was enlarged with increasing CO concentration in every case for the electrolyte-supported cells. It was reported that the polarization resistance for pure carbon monoxide fuel was almost the same as that in pure hydrogen fuel at a high temperature of 1273 K [15]. At a low temperature of 923 K, the rate of electrochemical oxidation of carbon monoxide is slower than that of hydrogen at low temperatures as shown in Fig. 3(a). On the other hand, the polarization resistance in CO–H_2O mixture (i and ii) was smaller than that in CO–CO_2 mixture (iii and iv) at x = 25 and 923 K for the electrolyte-supported cells. This result was caused by the

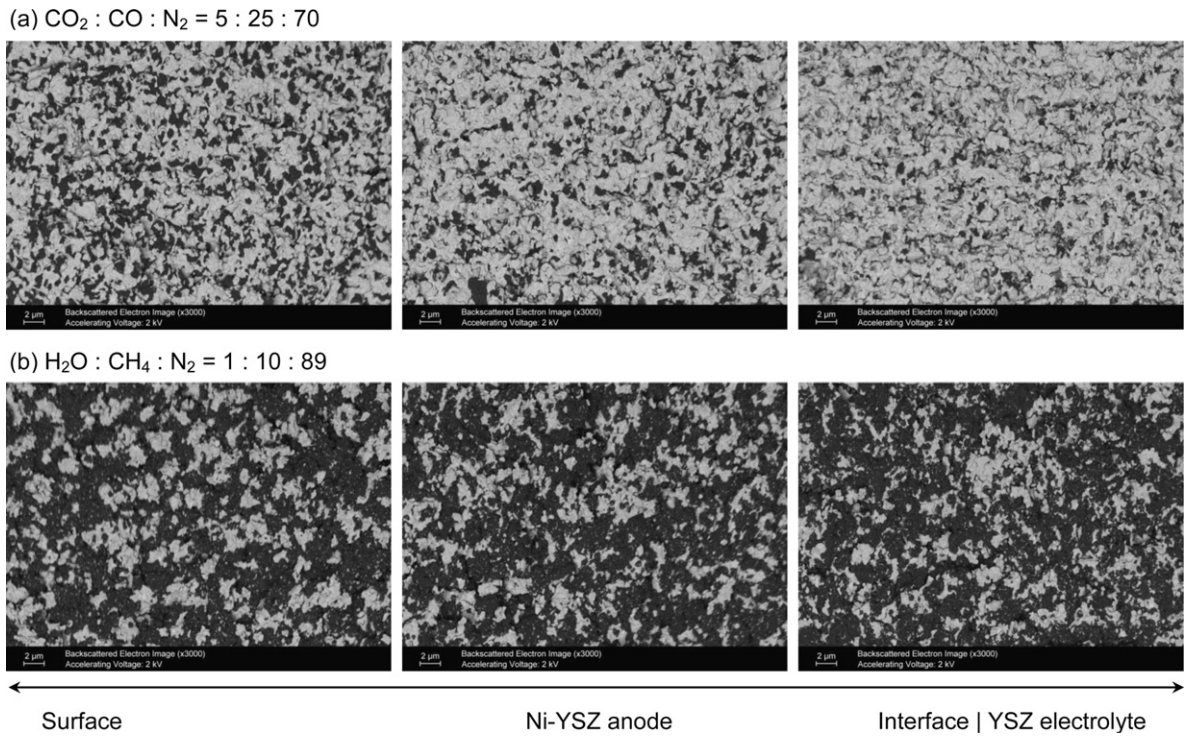

Fig. 6. Backscattered electron images for the Ni–YSZ anodes of the anode-supported cells after power generation for 20 h with supplies of (a) CO_2–CO mixture at 923 K and (b) H_2O–CH_4 mixture at 1073 K.

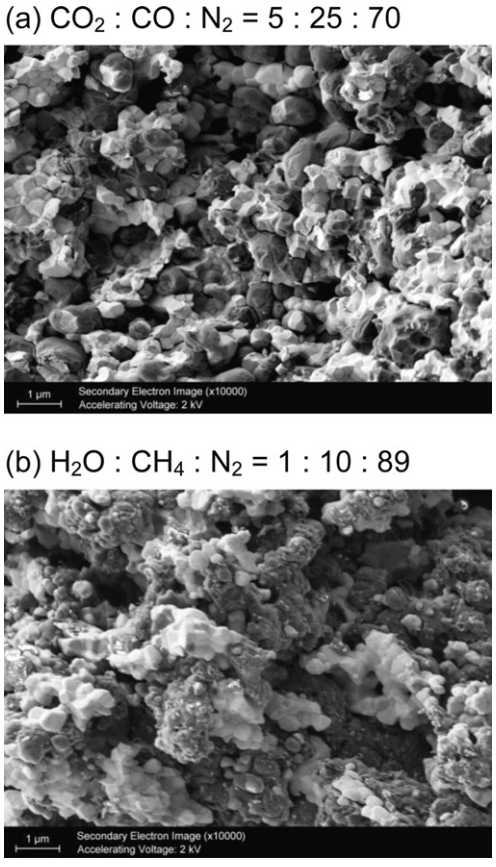

Fig. 7. Secondary electron images for the Ni–YSZ anodes of the anode-supported cells after power generation for 20 h with supplies of (a) CO_2–CO mixture at 923 K and (b) H_2O–CH_4 mixture at 1073 K.

promotion of water gas shift reaction and the decrease in the CO concentration.

$$CO + H_2O \leftrightarrow H_2 + CO_2 \quad \Delta H_{298\,K} = -41\,kJ\,mol^{-1} \tag{3}$$

For the anode-supported cells, the impedance spectra were almost unchanged against CO concentration in all conditions as shown in Fig. 3(b). The carbon deposition did not lead to increase in the polarization resistance. This result agreed well with similar slope of the *i*–*V* curves at low current density as shown in Fig. 2(b). Next, the compositions of anode exhaust gases at OCV and 62.5 mA cm^{-2} were analyzed with micro gas chromatography to investigate whether the water gas shift reaction proceeded. Table 1 shows the results of gas chromatography analysis and equilibrium calculation at $y = 3$ in H_2–CO–H_2O mixture, $y = 5$ in H_2–CO–CO_2 mixture and 923 K. The production of hydrogen and carbon dioxide are facilitated in equilibrium by forward reaction (3) with increasing CO concentration, *x*, in H_2–CO–H_2O mixture. On the contrary, the formation of steam and carbon monoxide are promoted by reverse reaction (3) with decreasing *x* in H_2–CO–CO_2 mixture. Furthermore, the carbon monoxide decreases and the carbon dioxide increases in the carbon deposition condition by the Boudouard reaction (1). Actually at OCV, the production of hydrogen at $x = 25$ in CO–H_2O mixture and that of carbon monoxide at $x = 0$ in H_2–CO_2 mixture confirmed the progress of water gas shift reaction. In addition, the Boudouard reaction also proceeded as evidenced by the increasing amount of carbon dioxide from the initial amount of 5 mL min^{-1} at $x > 16.7$ in H_2–CO–CO_2 mixture. The difference between the calculation and the experimental values at OCV increased with a rise in CO concentration. This result suggests that the rate of the Boudouard reaction was slower than that of water gas shift reaction at 923 K. Hydrogen and carbon monoxide are oxidized electrochemically under current loading.

$$H_2 + O^{2-} \rightarrow H_2O + 2e^- \tag{4}$$

$$CO + O^{2-} \rightarrow CO_2 + 2e^- \tag{5}$$

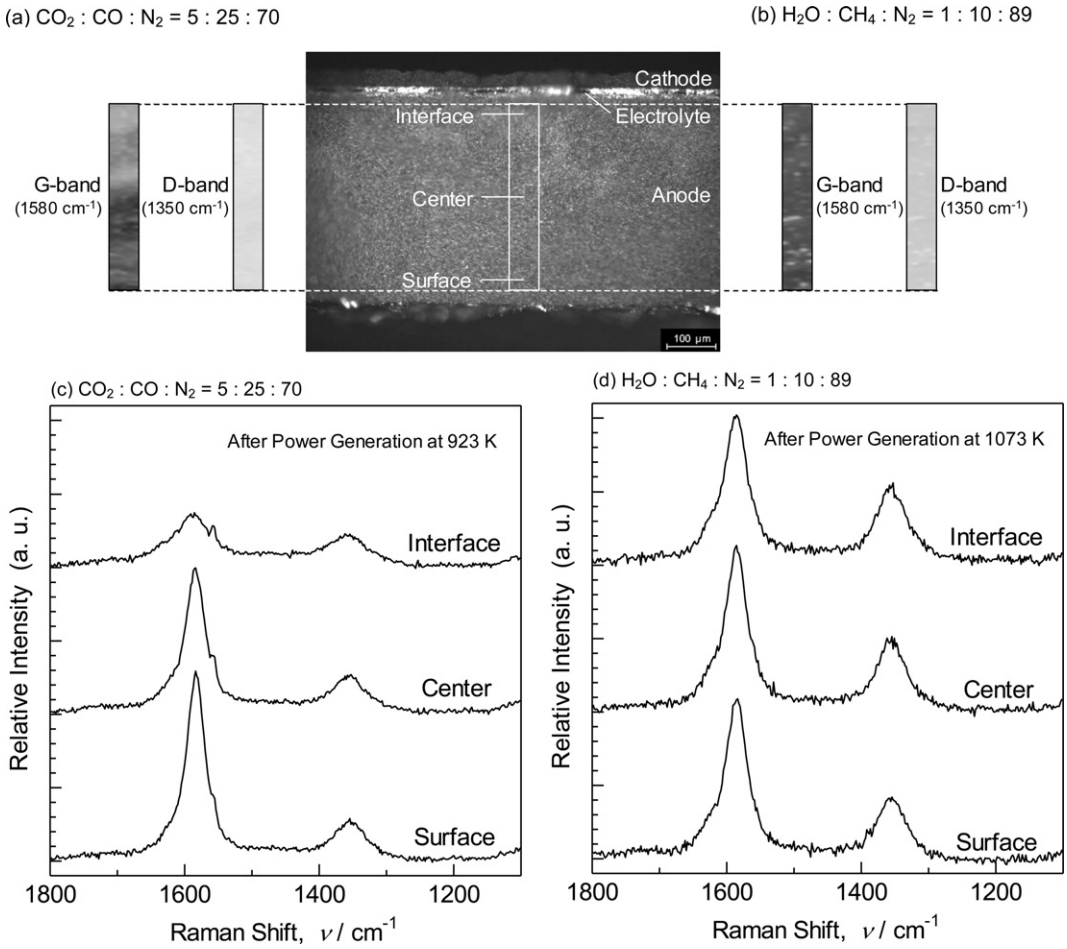

Fig. 8. Raman mapping image and spectra for the Ni–YSZ anodes of the anode-supported cells after power generation for 20 h with supplies of (a), (c) CO_2–CO mixture at 923 K and (b), (d) H_2O–CH_4 mixture at 1073 K.

The decrease in the sum of hydrogen and carbon monoxide was approximately 1 mL min^{-1} in all conditions under a current loading of 142 mA. This result agreed with the estimated consumption of 6.96 mL min^{-1} A^{-1} from Faraday's law by the reactions of (4) and (5). The H_2/CO ratio was almost unchanged experimentally with and without current loading in all conditions. Carbon monoxide was consumed by the electrochemical oxidation (5) and/or water gas shift reaction (3) at a low temperature of 923 K.

Next, the carbon deposition behavior was compared with methane cracking. Fig. 4 shows the *i*–*V* characteristics and ac impedance spectra for the (a) electrolyte- and (b) anode-supported cells at 1073 K with supplies of H_2O–H_2 and H_2O–CH_4 mixtures. The impedance for the electrolyte-supported cell in Fig. 4(a) was measured between the anode and reference electrode as well as in Fig. 3(a). Carbon is expected to be deposited at S/C < 1 and 1073 K in equilibrium. The OCV value in H_2O–CH_4 mixture was larger than that in H_2O–H_2 mixture because of the decrease in oxygen partial pressure in the carbon deposition condition. The slopes of *i*–*V* curves became steep at low current density arcs in H_2O–CH_4 mixture. The impedance arcs in H_2O–CH_4 mixture were larger than that in H_2O–H_2 mixture for both of the cells. This result was different from no change of impedance spectra in CO_2–CO mixture for the anode-supported cells in Fig. 3(b). The slopes at high current density in H_2O–CH_4 mixture was steeper than that in H_2O–H_2 mixture for the anode-supported cells, which supposed the increase in diffusion resistance of methane as well as carbon dioxide in the thick anode layer.

Durability tests were conducted to investigate carbon deposition behavior precisely. Fig. 5 shows the time courses of cell voltage for the (a) electrolyte- and (b) anode-supported cells with supplies of CO_2–CO mixture at 923 K and H_2O–CH_4 mixtures at 1073 K. The cell voltage decreased rapidly for the initial 10–60 min in H_2O–CH_4 mixture for both of the cells, followed by the voltage gradual decrease. On the other hand, the voltage continuously decreased in CO_2–CO mixture. This result suggests that the rate of carbon deposition in H_2O–CH_4 mixture is different from that in CO_2–CO mixture.

The Ni–YSZ anodes after durability test were observed with FE-SEM and Raman spectroscopy. Fig. 6 shows the backscattered electron images of the cross-section for the anode-supported cells after power generation for 20 h in (a) CO_2–CO mixture at 923 K and (b) H_2O–CH_4 mixture at 1073 K. The black areas were ascribed to the deposited carbon, which was confirmed by an energy-dispersive X-ray spectrometer. Although a large amount of carbon was deposited near the anode surface after power generation in CO_2–CO mixture, less amount of carbon was observed near the interface between the anode and the electrolyte. This result suggests that the Boudouard reaction (1) proceeds only near the anode surface. On the other hand, the large amount of deposited carbon was observed from the anode surface to the anode/electrolyte interface after power generation in H_2O–CH_4 mixture, which supported the methane cracking reaction (2) proceeded in the whole anode layer. These results also propose that the reaction rate of methane cracking at 1073 K is slower than that of CO disproportionation at 923 K. Fig. 7 shows the secondary electron images

of the Ni–YSZ anodes near the surface after power generation for 20 h in (a) CO_2–CO mixture at 923 K and (b) H_2O–CH_4 mixture at 1073 K. The deposited carbon as the coated layer on the nickel particles was observed after power generation in CO_2–CO mixture. However, the agglomerated cokes were deposited after power generation in H_2O–CH_4 mixture. The carbon with a similar morphology was observed after power generation at 1273 K and S/C = 0.5 in methane fuel [15]. The morphologies of deposited carbon for the electrolyte-supported cells were almost the same as that for the anode-supported cells. As the anode layer was thinner for the electrolyte-supported cells, the deposited carbon was confirmed from the anode surface to the anode/electrolyte interface after power generation in CO_2–CO mixture. The polarization resistance of the anode became large in the carbon deposition conditions except in CO_2–CO mixture for the anode-supported cells, which had no deposited carbon in the vicinity of the anode/electrolyte interface. Therefore, the increase in polarization resistance strongly correlated with the carbon deposition near the anode/electrolyte interface.

Raman spectra were measured to investigate the local structure and distribution of deposited carbon. Fig. 8 shows the mapping images and spectra for the Ni–YSZ anodes of the anode-supported cells after power generation for 20 h in (a), (c) CO_2–CO mixture at 923 K and (b), (d) H_2O–CH_4 mixture at 1073 K. The peaks at *ca.* 1350 cm^{-1} (D-band) and *ca.* 1580 cm^{-1} (G-band) are attributed to amorphous carbon and crystalline graphite, respectively. The mapping images for the intensities of D-band and G-band were taken at 5 μm intervals in the area of 20 μm in width × 400 μm in height. The stronger the peak intensity is, the darker mapping images become in Fig. 8(a) and (b). While the peak intensity of G-band was strong near the anode surface, the intensity was weak in the vicinity of the anode/electrolyte interface after power generation in CO_2–CO mixture. This result agrees with the distribution of deposited carbon observed with FE-SEM as shown in Fig. 6(a). The strong peaks of G-band were observed from the anode surface to *ca.* 200 μm in depth, which resulted from the occurrence of CO disproportionation during the durability test for 20 h in this region. The peak intensity of D-band was weak in the whole anode layer. The carbon was deposited as coating layer on the nickel particles as shown in Fig. 7(a) was attributed to crystalline graphite. On the other hand, the peak intensities of D-band and G-band were unchanged throughout the anode layer after power generation in H_2O–CH_4 mixture. This result also agrees with the wide distribution of deposited carbon observed with FE-SEM as shown in Fig. 6(b). The intensity ratio of D-band/G-band after power generation in H_2O–CH_4 mixture was larger than that in CO_2–CO mixture. The agglomerated cokes as shown in Fig. 7(b) contained the large amount of amorphous carbon. The distribution in deposited carbon as shown in Fig. 8 suggests that the rate of methane cracking at 1073 K is slower than that of CO disproportionation at 923 K. The deposited carbon near the anode/electrolyte interface affected strongly the increase in the polarization resistance.

4. Conclusion

In this study, the cell performance and ac impedance were evaluated at 923 K and as a function of H_2/CO ratios in H_2–CO–H_2O and H_2–CO–CO_2 mixtures, and carbon deposition behavior by carbon monoxide disproportionation and methane cracking was compared. The polarization resistance was enlarged with increasing CO concentration for the electrolyte-supported cells. This result suggests that electrochemical oxidation of carbon monoxide is more difficult than that of hydrogen at low temperatures. The polarization resistance in H_2–CO–H_2O mixture was smaller than that in H_2–CO–CO_2 mixture because of the decrease in CO concentration by water gas shift reaction. While the polarization resistance was unchanged in CO_2–CO mixture for the anode-supported cells, the resistance increased in H_2O–CH_4 mixture for both of the cells in the carbon deposition condition. The graphite was deposited as coated layer on the nickel particles only near the anode surface facing to the flowing gas after durability test in CO_2–CO mixture for the anode-supported cells. On the other hand, a large amount of agglomerated amorphous carbon was deposited from the anode surface to the interface between the anode and the electrolyte after power generation in H_2O–CH_4 mixture. These results suggest that the rate of methane cracking at 1073 K was slower than that of CO disproportionation at 923 K. It was concluded that the increase in polarization resistance was strongly correlated with the carbon deposition near the anode/electrolyte interface.

References

[1] J. Yan, H. Matsumoto, M. Enoki, T. Ishihara, Electrochem. Solid-State Lett. 8 (2005) A389–A391.
[2] B.C.H. Steele, Solid State Ionics 129 (2000) 95–110.
[3] T. Hibino, A. Hashimoto, T. Inoue, J. Tokuno, S. Yoshida, M. Sano, Science 288 (2000) 2031–2033.
[4] Z. Shao, S.M. Haile, J. Ahn, P.D. Ronney, Z. Zhan, S.A. Barnett, Nature 435 (2005) 795–798.
[5] T. Suzuki, Z. Hasan, Y. Funahashi, T. Yamaguchi, Y. Fujishiro, M. Awano, Science 325 (2009) 852–854.
[6] T. Suzuki, T. Yamaguchi, Y. Fujishiro, M. Awano, J. Electrochem. Soc. 153 (2006) A925–A928.
[7] T. Suzuki, T. Yamaguchi, Y. Fujishiro, M. Awano, J. Power Sources 160 (2006) 73–76.
[8] K. Eguchi, H. Kojo, T. Takeguchi, R. Kikuchi, K. Sasaki, Solid State Ionics 152–153 (2002) 411–416.
[9] H. Sumi, K. Ukai, Y. Mizutani, H. Mori, C.-J. Wen, H. Takahashi, O. Yamamoto, Solid State Ionics 174 (2004) 151–156.
[10] A. Gunji, C. Wen, J. Otomo, T. Kobayashi, K. Ukai, Y. Mizutani, H. Takahashi, J. Power Sources 131 (2004) 285–288.
[11] K. Ke, A. Gunji, H. Mori, S. Tsuchida, H. Takahashi, K. Ukai, Y. Mizutani, H. Sumi, M. Yokoyama, K. Waki, Solid State Ionics 177 (2006) 541–547.
[12] T. Matsui, T. Iida, R. Kikuchi, M. Kawano, T. Inagaki, K. Eguchi, J. Electrochem. Soc. 155 (2008) B1136–B1140.
[13] K. Yamaji, H. Kishimoto, Y. Xiong, T. Horita, N. Sakai, M.E. Brito, H. Yokokawa, Solid State Ionics 179 (2008) 1526–1530.
[14] M.B. Pomfret, J. Marda, G.S. Jackson, B.W. Eichhorn, A.M. Dean, R.A. Walker, J. Phys. Chem. C 112 (2008) 5232–5240.
[15] H. Sumi., Y.-H. Lee, H. Muroyama, T. Matsui, K. Eguchi, J. Electrochem. Soc. 157 (2010) B1118–B1125.
[16] M. Audier, M. Coulon, L. Bonnetain, Carbon 17 (1979) 391–394.
[17] J. Guinot, M. Audier, M. Coulon, L. Bonnetain, Carbon 19 (1981) 95–98.
[18] E.G.M. Kuijpers, A.J.H.M. Kock, M.W.C.M. Nieuwesteeg, J.W. Geus, J. Catal. 95 (1985) 13–20.
[19] C. Mirodatos, H. Praliaud, M. Primet, J. Catal. 107 (1987) 275–287.
[20] P.E. Nolan, D.C. Lynch, A.H. Cutler, Carbon 32 (1994) 477–483.
[21] J. Jiao, P.E. Nolan, S. Seraphin, A.H. Cutler, D.C. Lynch, J. Electrochem. Soc. 143 (1996) 932–935.
[22] K. Tomishige, Y.-G. Chen, K. Fujimoto, J. Catal. 181 (1999) 91–103.
[23] K. Sasaki, Y. Hori, R. Kikuchi, K. Eguchi, A. Ueno, H. Takeuchi, M. Aizawa, K. Tsujimoto, H. Tajiri, H. Nishikawa, Y. Uchida, J. Electrochem. Soc. 149 (2002) A227–A233.
[24] A. Weber, B. Sauer, A.C. Müller, D. Herbstritt, E. Ivers-Tiffee, Solid State Ionics 152–153 (2002) 543–550.
[25] V. Alzate-Restrepo, J.M. Hill, J. Power Sources 195 (2010) 1344–1351.